ACS APPLIED OPTICAL MATERIALS

pubs.acs.org/acsaom Article

Efficient, Hydrophobic, and Weather-Resistant Radiative Cooling Paints with Silicone-Based Binders

Emily Barber, Dudong Feng, Ziqi Fang, Daniel Carne, Orlando Rivera Gonzalez, Won-June Lee, Navdeep Vansal, Katherine Raykova, and Xiulin Ruan*

Cite This: https://doi.org/10.1021/acsaom.5c00079 Read Online

ACCESS | Metrics & More | Article Recommendations | Supporting Information

ABSTRACT: Radiative cooling technology has gained significant interest, in large part due to the discovery of passive subambient cooling without any external energy input. These technologies, while pertinent in the areas of climate change and heating, ventilation, and air conditioning (HVAC) efficiency, have encountered unique issues, including dampening of their effects over time due to soiling and UV weathering. This study advances passive radiative cooling paint technology through the incorporation of MP-101, a silicone-based binder developed by SDC Inc., into hBN-based radiative cooling paints. The introduction of MP-101 enhances the durability of these paints, addressing issues related to contamination and ultraviolet radiation. The newly formulated paint exhibits an ultrahigh solar reflectance of 97.8%, an average temperature reduction of 1.97 °C in West Lafayette, IN, USA, and a hydrophobic surface with a static contact angle of 142° without any topcoats, implying improved self-cleaning capabilities compared to previous hBN formulations. Comprehensive investigations into abrasive properties, pigment loading percentages, cooling performance, and UV exposure demonstrated the optimization of the formula's durability and cooling performance. The self-cleaning feature not only preserves optical properties over time but also extends the applicability of the paint to diverse settings, including buildings, transportation, and outdoor electronic systems, with reduced maintenance requirements and the highest known reflectance of hydrophobic radiative cooling materials.

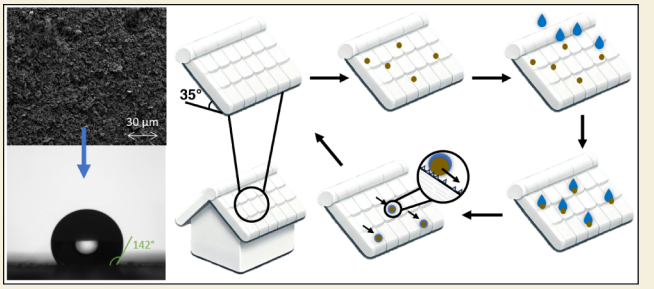

KEYWORDS: *radiative cooling, self-cleaning, hydrophobic, coatings, surface science, climate change*

INTRODUCTION

In 2015, air conditioning accounted for around 12% of total energy costs for residential buildings in the USA,[1] and in 2021, around 61% of this energy came from fossil fuels.[2] Therefore, as the energy sector shifts to mitigate the effects of climate change, attention has been brought to the reduction of HVAC demand. One promising way to encourage this reduction is by switching cooling needs from the current form of active cooling, where energy input is required, to passive cooling, which uses no energy input. Radiative cooling (RC) relies on both high emissivity within the "sky window" (8−13 μm) and high solar reflectance, enabling materials to cool below ambient temperature if more energy is lost through these methods than absorbed from solar irradiation. There is a history of people cooling their houses by painting their roofs white and creating ice in above-freezing temperatures.[3,4] Formal scientific studies of radiative cooling, however, started in the 1970s: the impact of dual-layer aluminum and TiO_2/PVF surfaces was quantified, and daytime below-ambient cooling was reported on winter days, with a notable boost in reflectance from the metal substrate instead of the paint alone.[5,6] More recently, a seven-layer HfO_2 and SiO_2 compound on Ag substrate was developed that reflected 97% of solar irradiation and cooled almost 5 °C below ambient temperatures.[7] Another approach using a polymer-coated fused silica mirror demonstrated full daytime subambient cooling of as much as 8.4 °C.[8]

RC researchers have also attempted scalable and paintable technologies without relying on metal substrates. Earlier experiments and simulations have demonstrated partial-daytime radiative cooling in dual-layer coatings and predicted the feasibility of full daytime cooling in TiO_2 dual-layer paints without a metal substrate.[9,10] A single-layer porous polymer, which relied on the high reflectance coefficient between the polymer and air, allowed for a subambient temperature drop of 6 °C and a reflectance of 96%.[11] Additionally, a randomized bed of SiO_2 particles was developed and achieved partial daytime subambient cooling.[12] Three single-layer paints based on commercial fabrication have been made at Purdue

Received: March 3, 2025
Revised: April 21, 2025
Accepted: April 21, 2025
Published: May 6, 2025

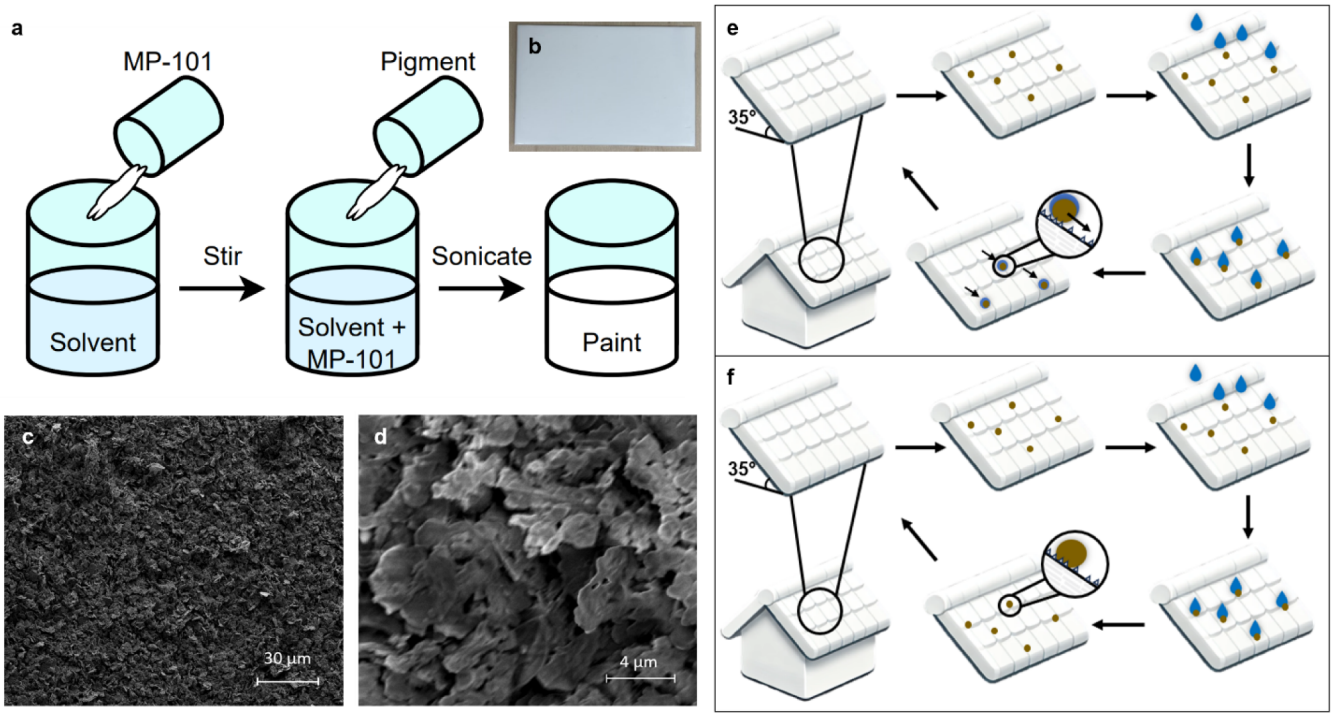

Figure 1. An introduction to self-cleaning radiative cooling paint. (a) A schematic of how the paint is formulated, including a simple process involving only stirring and sonication. (b) A picture of a finished paint sample. (c,d) SEM images showing the texture of the surface for an 80% loaded sample. (e) A hydrophobic roof versus a (f) hydrophilic roof and how rain impacts the debris left on their surfaces.

University: $CaCO_3$, $BaSO_4$, and hBN based paints with 95.5%, 98.1%, and 97.9% reflectance, respectively.[13−15] The hBN paint achieved this reflectance at much smaller thicknesses (150 μm) than previous formulas (~400 μm).[15]

Despite the demonstration of these low-cost, widely applicable, subambient RC paints, open questions remain over the durability of radiative cooling paints in the outdoor environment. Paints based on the conventional TiO_2 pigment were found to have their reflectance values decline by around 9% after the equivalent of 3 years of soiling and 5.4% after the equivalent of 1 year of Florida sunshine.[16] Additionally, a 20% reduction in reflectance was found for a hydrophilic surface after only a year of use for a cooling surface due to weathering and debris.[17] This is a common concern, with many high-reflectance cool roof technologies losing 10−20% reflectance after 3 years.[18] Although cleaning the paint, while not cost-effective, could restore its original properties, it is desirable to develop a dirt-resistant, durable, high-albedo coating.[17] Some previous studies have focused on hydrophobic/self-cleaning radiative cooling paints and made significant progress in introducing hydrophobicity while maintaining RC properties. Notably, Liu et al. used hBN in a PFOTS binder, and while it demonstrated excellent hydrophobic performance, the reflectance decreased to 96.3% and reflectance in the UV range showed degradation after 10 days of exposure.[19] Other studies on hydrophobic RC surfaces also present one or more limitations, including a reduced solar reflectance of less than 95%;[20−26] a lack of scalability due to a multilayer structure, complex/toxic materials, or complicated fabrication process;[22−30] or insufficient understanding of their durability.[20,23]

To attempt to address this gap, this paper introduces a single-layer, self-cleaning, durable formulation of paint using MP-101, a silicone-based binder produced by SDC Technologies, Inc. The MP-101 binder exhibits optical properties comparable to or slightly superior to the commonly used acrylic, with a solar absorptance of 0.6% compared to 1.1% for acrylic for a pure film of 50−80 μm thickness. This decreased absorption facilitates effective radiative cooling by allowing incoming radiation to interact with the highly reflective hBN pigment and be rejected from the surface. A sample with 80% pigment solid volume loading achieved a total reflectance of 97.8%, which, considering error, is comparable to the hBN-acrylic formulation's 97.9% reflectance. The paint's hydrophobic nature, with a static water droplet contact angle of approximately 143° and an advancing angle of 155°, is expected to create antisoiling properties through the petal effect. Moreover, pigment loading analysis demonstrated that 52% solid volume concentration of hBN MP-101 maintains strength comparable to previous hBN acrylic paints, with only a 1% reduction in reflectance from the peak value of 97.8%. Field tests showed full daytime subambient temperatures. Additionally, solar weathering tests showed no noticeable degradation of the paint's reflectance after solar exposure, providing potential for better long-term performance than acrylic paints. Therefore, this formula demonstrates the desired self-cleaning ability without substantial compromise to the paint's overall strength or cooling ability.

RESULTS AND DISCUSSION

In this work, SDC's polysiloxane-based polymer MP-101 was tested as a binder for radiative cooling paints in place of the standard acrylic used in many paint-based applications.[6,10,13,14,31] MP-101, originally formulated for contact lenses, has high optical clarity and durability both to abrasion and outdoor elements. Following testing, MP-101 was proven to have minimal impact on the optical properties that are required for radiative cooling while also creating a hydrophobic

https://doi.org/10.1021/acsaom.5c00079
ACS Appl. Opt. Mater. XXXX, XXX, XXX−XXX

formulation that allowed for a strong self-cleaning paint with no observable degradation due to solar exposure.

To first understand how this paint is formulated, Figure 1a is provided to show the simple process involving stirring and sonication that suspends the hBN nanoparticles in the MP-101 matrix. hBN was used due to its high reflectance as well as its low density and thickness that allows it to be applied to more applications than a typical RC paint.[15] Figure 1b shows the finished product on a glass slide. Additionally, SEM images were taken of the 80% loaded paint, as shown in Figure 1c,d. The SEM images show that the surface of the paint is very rough and textured at the microscale. Additional SEM images showing this roughness for a 91% loaded sample can be found in Figure S1. The paint's roughness is supported by a paint porosity of 74%, which was determined using the volume displacement method to calculate the density of the dried paint layer and MP-101. In **Figure** 1e,f, we show a diagram of two roofs being coated with debris over time and what happens to that debris when it rains. For a hydrophobic surface (Figure 1e), the roof's low surface energy/repelling of water encourages water to stay "on top" of the surface and easily flow off, carrying debris with it. For a hydrophilic surface (Figure 1f), the water is trapped on the surface, soaking into the texture on its surface and slowing down or stopping the water movement, thereby discouraging debris removal.

Table 1 displays spectral results normalized over AM 1.5 (ASTM G-173) solar data from plain MP-101 and acrylic, poured onto a glass slide, and measured using a UV−Vis−NIR spectrometer. This normalization was completed by taking a weighted average of each reflectance data point with respect to the magnitude of the AM 1.5 data. The lack of pigment in these films means that a high reflectance is not anticipated: instead, an ideal binder would have minimal absorptance so that once a pigment is added, the chosen binder has minimal interference with the pigment's optical properties. Here it was observed that the acrylic's total solar absorptance is 1.1%, while the MP-101's total solar absorptance was 0.6%, indicating both to be excellent binder materials with minimal absorption and MP-101 as a potentially better choice. The optical properties across the solar spectrum for these nonpigmented films are shown in Figure S2.

Table 1. Total Solar Reflectance, Transmittance, and Absorptance of Pure Acrylic and MP-101 Films of 1.27 mm Thickness

	Reflectance	Transmittance	Absorptance	Emittance
Acrylic	7.9%	91.1%	1.1%	0.92
MP-101	7.3%	92.1%	0.6%	0.92

The spectral optical properties of a mixture of MP-101 and hBN pigment particles with an 80% pigment volume loading are shown in Figure 2a. It was found that this formulation had a high reflectance (>95%) for a majority of the solar spectrum, with some of the highest values across the visible spectrum and the lowest values around 2−2.5 μm, where there is minimal solar irradiation (as shown by the AM 1.5 data on the plot). This is supported by the similar refractive indices (n) of acrylic and MP-101 as shown in Figure 2b. Additionally, the emission within the sky window (8−13 μm) measured using an FTIR spectrometer is reasonably high (0.81), although not as high as the 60% loaded acrylic formulation's emission of 0.83,[15] despite plain MP-101 and acrylic having around the same emittance of 0.92, as shown in Table 1. For both acrylic and MP-101, the extinction coefficient shown in Figure 2b was highest in the sky window while being generally low in the solar spectrum. This allows for the similarly high absorptance and emission observed in the sky window for both binders. Emission values for additional pigment loadings can be found in Table S1. Considering the error, the reflectance value of 97.8% is comparable to previous results for hBN acrylic paints (97.9%)[15] due to the similarly low absorptance of acrylic and MP-101 binders as shown in Table 1. Spectrometry measurements for additional pigment loadings can be found in Figure S3. Additional spectrometry testing was also done on a two-layer formulation that utilized a topcoat of MP-101 to further increase the hydrophobicity. This ultimately decreased the reflectance of the sample, and the results are presented in Figure S4.

The surface wettability of the 80% pigment-loaded paint was characterized through both static and dynamic testing, as shown in Figure 2c. For static testing, the interior droplet angle was measured by spreading a sample of paint onto a glass substrate. After drying, dynamic testing was completed by slowly adding water to the surface in 5 μL increments until the point at which the edge of the drop touching the surface changed. At this point, the advancing angle was recorded as the angle that the waterdrop makes with the surface from the interior. Then, the water was removed in 5 μL increments until the edge of the water droplet contact point changed once again—at this point, the receding contact angle was measured in the same way as the advancing angle. The new formulation's final contact angle for the static droplet was calculated as 142°, the final for the advancing drop was 155°, and the final for the receding drop was 25°. Surfaces are defined as hydrophobic when their contact angle surpasses 90°; therefore, the hBN-MP 101 paint formulation is highly hydrophobic, enabling its self-cleaning capabilities. Additionally, a measured contact angle hysteresis of around 120°, combined with the surface roughness characterized in Figure 2c,d, alludes to the presence of the petal effect[32]—a surface phenomenon (also called the Cassie−Baxter state) that encourages hydrophobicity and discourages movement along the surface, as opposed to the more commonly known lotus effect. Both effects are demonstrated in Figure 2d. It is important to mention that due to the presence of the petal effect and not the lotus effect, this hydrophobicity will likely only lead to self-cleaning when the surface is at an angle—but the lotus effect would also require an angle of some degree, and most of the roofs also provide the angle needed. Additionally, the Supporting Information shows that once this angle is provided, water easily removes debris from the surface.

Once the initial samples were tested above, a pigment loading study was performed on the new formulation. The paint's mechanical strength at different pigment loadings was tested using the Taber Abraser by measuring the weight of dried samples on a circular aluminum substrate after every 250 abrasion cycles, with consistent abrasion maintained by sanding the pads every 500 cycles. The abrasion testing data are shown at different pigment loadings in Figure 3a. It is expected that as pigment loading decreases, the strength of the paint increases as there is more binder to hold the paint together. However, this is not what we observed: the highest perceived volume loss occurred in the 73% pigment loading sample. It is hypothesized that this is a testing error, as the largest pigment loadings lost most of their volume quickly

https://doi.org/10.1021/acsaom.5c00079
ACS Appl. Opt. Mater. XXXX, XXX, XXX−XXX

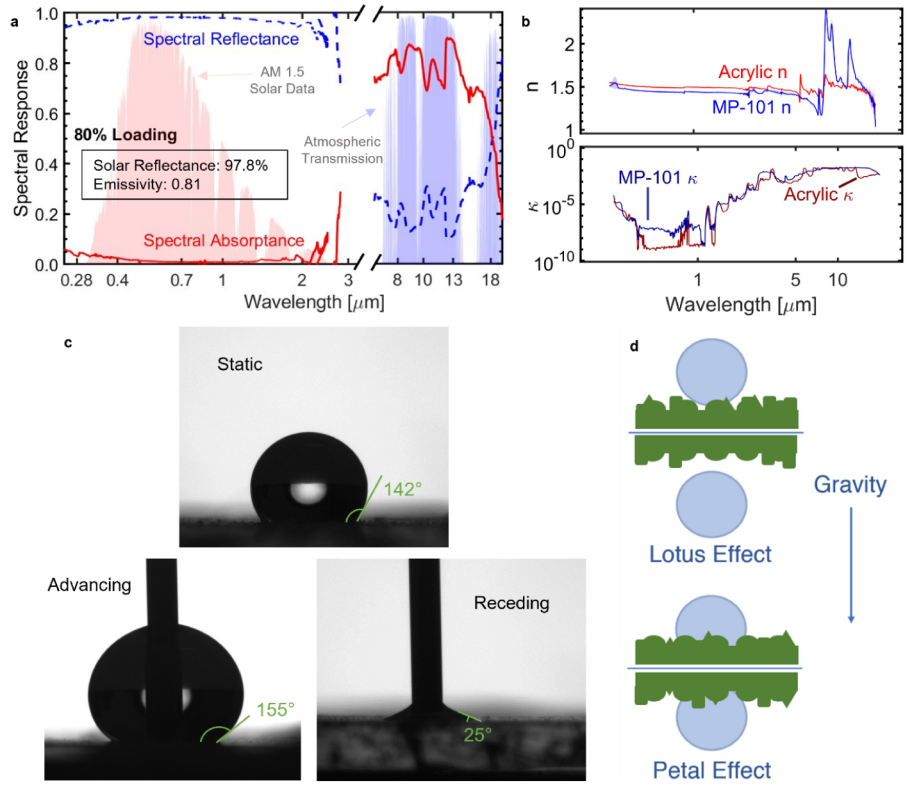

Figure 2. Characterization of MP-101 + hBN formulation with an 80% pigment loading. (a) The reflectance and absorptance characterization of the paint through UV−vis−NIR and FTIR spectrometry. (b) The refractive index [n] and extinction coefficient [κ] of MP-101 is compared to commonly used acrylic, with the shading representing error, most clearly at the edges of the n data. (c) The static, advancing, and receding contact angles of the loaded paint. (d) Explanation of the petal and lotus effects, both of which can result from a rough surface.

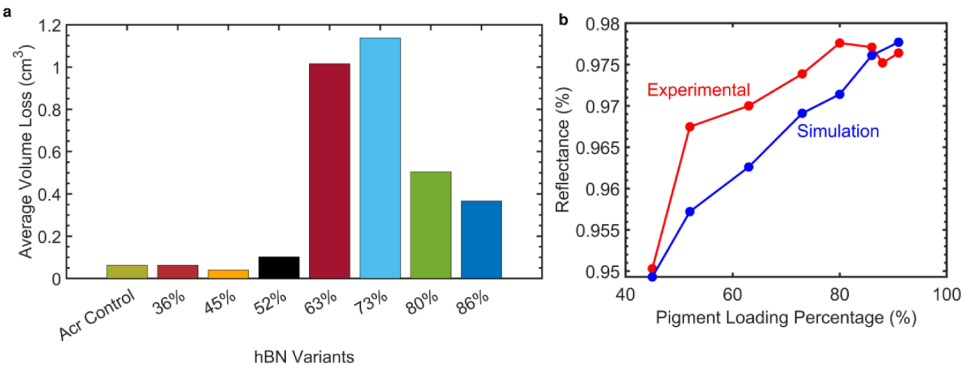

Figure 3. Pigment loading optimization for the new formula. (a) Strength of the different pigment loadings, measured in average volume loss due to the abrasion normalized to the density of the paint. (b) Experimental and simulation-based reflectance characterization depending on the pigment loading percentage.

through chipping. This hypothesis is supported by the fact that the largest pigment loadings have much larger volume loss earlier in the test, which decrease as the number of cycles increases. Regardless, it was still found that to achieve a similar cohesion strength to an acrylic paint with 60% loading, the pigment loading had to be around 52%. Therefore, the paint requires slightly more binder than an acrylic formulation to function at the same strength.

The modeled and experimental solar reflectances as a function of the pigment volumetric loading are shown in Figure 3b[a]. For the model, the scattering coefficient and asymmetry parameter were first calculated by directly solving Maxwell's equations using the finite element method in COMSOL. Next, the effective scattering coefficient and absorption coefficient for the medium were calculated by volume averaging the hBN platelets with the MP-101 matrix based on the filling fraction. Finally, the Monte Carlo method stochastically modeled photon packets' transport through the paint to calculate the spectral response. For both the modeling and experimental cases, the reflectance of the formulation is still high at lower measured pigment levels, with an experimentally measured reflectance of 96.8% at a 52% pigment loading, which is still comparable to some of the most reflective RC materials at a similar strength. The experimental and simulation results more accurately match around the middle pigment levels. However, the general shape of the graphs as well as the approximate reflection match as

https://doi.org/10.1021/acsaom.5c00079
ACS Appl. Opt. Mater. XXXX, XXX, XXX−XXX

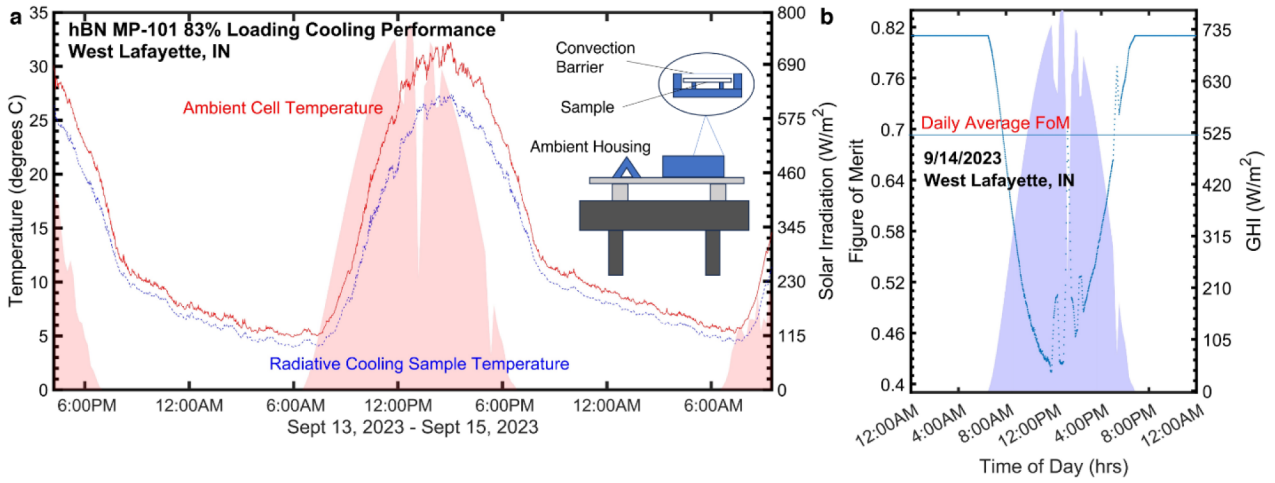

Figure 4. Outdoor testing results and their calculated figure of merit. (a) Outdoor testing from 9/13/2023 to 9/15/2023 in West Lafayette, IN, which displayed full subambient cooling over a 24-h period with a 5-min running average. (b) Time-dependent FoM for this outdoor testing over a 24-h period with a 5-min running average, as well as the average dFoM. FoM is shown to be inversely correlated to GHI.

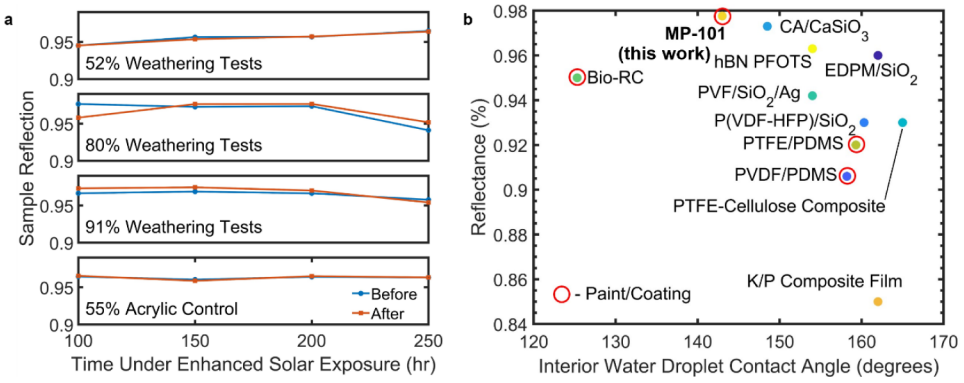

Figure 5. Weathering test results and a comparison of MP-101 to current hydrophobic RC paint literature. (a) Durability analysis for the hBN MP-101 formulation through accelerated solar irradiation testing. (b) How the new formulation compares to previous literature on self-cleaning paints focusing on hydrophobicity as well as their final reported reflectance.[19−25,27−30]

expected. The exact measurements for the experimental data can be found in Table S2.

In Figure 4a, the cooling performance of the paint was tested through an outdoor test using a chamber with a convection shield at the top. Outdoor testing was completed on the roof of Herrick Laboratories in West Lafayette, IN, USA. With a running average time of 5 min, the sample exhibited full 24-h subambient cooling over the testing period compared to an ambient thermocouple within the cell. The results exhibit similar cooling during the day and night, unlike most results, which show higher cooling at night. This is because of the use of the ambient cell, which experiences a localized cooling/heating effect due to its proximity to the white paint and limited convection. The main conclusion from this graph, however, is the 100% subambient temperature, with an average temperature reduction of 1.97 °C. Results using a sidewall wind shield and open top, as opposed to an enclosed chamber, are shown in Figure S5 and demonstrate 100% subambient cooling within the cell with a 5-min running average, although with more variation likely due to increased convection. GHI numbers shown on the right-hand *y*-axis were recovered from the NSRDB tool developed by the National Renewable Energy Laboratory (NREL).[33] This tool predicts a typical meteorological year (tmy) through many sources, including multiple satellites, and includes potential coverage by clouds/debris. However, it is not the same as the solar irradiation observed directly at the experimental site in 2023; it is just provided as an estimate to provide context about what is expected during that time of year.

In ref 12, a figure of merit (FoM) was created to understand the daytime performance of an RC material, i.e., during noon hours under peak solar irradiance. In this paper, we propose a slightly alternate "daily" figure of merit (dFoM) that seeks to understand how an RC material creates an impact over a 24-h period, better capturing the perceived effects of reflectance, emission, and impact of temperature. To do this, the FoM from ref 12 is first restated in eq 1

$$\mathrm{RC} = \epsilon_{\mathrm{sky}} - r(1 - R_{\mathrm{solar}}) \tag{1}$$

where ϵ_{sky} is the sky window emissivity, R_{solar} is the reflectance in the solar spectrum, and $r = G/E$ (solar irradiation power/blackbody surface emissive power transmitted through the sky window). When discussing a dFoM as opposed to an instantaneous one, we begin to vary G and T (where T exists inside the integral of E) by each minute instead of assuming them to be constant. Then, an average is taken over a 24-h period to find the final dFoM. The dFoM for this formulation was calculated from the outdoor testing to be 0.69, and the FoM for each minute can be seen in Figure 4b. Additionally, it

https://doi.org/10.1021/acsaom.5c00079
ACS Appl. Opt. Mater. XXXX, XXX, XXX−XXX

is worth noting that RC times the blackbody surface emissive power in the sky window can estimate the net cooling power of the paint. For ∼300 K, the blackbody surface emissive power is around 96.5 W/m^2, so this means we can estimate that this paint has a maximum cooling power of approximately 78.2 W/m^2 and a daily cooling power average of 66.6 W/m^2.

To understand the long-term performance of the new formulation, the results of an advanced weathering experiment are shown in Figure 5a. For this weathering test, ISO 11341, Cycle A, Method 1 was used with a Q-SUN XE-3 instrument to test paint samples at different exposure increments (100, 150, 200, and 250 real-time hours) using a filter that allowed incoming radiation to mimic that of natural sunlight, although at an enhanced intensity. Notably, no significant signs of degradation beyond an expected margin of error of approximately 1% R were observed for any sample, including 52%, 80%, and 91% hBN MP-101, as well as a control sample of 55% hBN acrylic formulation. This verified that the MP-101 hBN formulation will not degrade quickly due to solar exposure, demonstrating more promising durability. Exact data for this experiment can be found in Table S3.

It is also important to note that there have been multiple other hydrophobic formulations proposed for radiative cooling paints. In Figure 5b, our work's hydrophobic and RC capabilities are compared to previous literature published on this topic. We focus on reflectance instead of emissivity due to the larger impact of reflectance in the dFoM defined above. It can be noted that very few of the proposed formulations are easily applied single-layer paints. Additionally, compared to the available literature, the hBN MP-101 formulation has the highest reflectance while remaining comfortably hydrophobic and, therefore, self-cleaning.

CONCLUSION

The emergence of radiative cooling paints as a promising solution to help mitigate climate change emphasizes the need for studying and optimizing their durability for commercial viability. In this study, we developed a new paint formulation utilizing SDC Technology's MP-101 polymer as a binder and nanoparticle hBN as a pigment. This formulation maintained ultrawhite cooling capability while incorporating hydrophobicity for self-cleaning properties. The optical properties of the MP-101 binder alone were comparable to or slightly better than those of the commonly used acrylic, with a solar absorptance around 0.5% lower. This low absorption combined with high emission allowed for an effective radiative cooling by reflecting the incoming radiation away from the surface. An 80% pigment loading sample of the new formulation exhibited a total reflectance of 97.8%, which, when considering error, is the same as that of an hBN acrylic formulation. The hydrophobic nature of the paint, with a static water droplet contact angle of around 143°, is shown to produce antisoiling properties, facilitating self-cleaning through the petal effect. Analysis showed that a 52% hBN MP-101 loading yielded a comparable strength to previous hBN acrylic paints, with only a minimal sacrifice in reflectance. Furthermore, weathering tests demonstrated no noticeable reduction in reflection for the new formulation, potentially demonstrating a longer durability than acrylic formulations. Additionally, the new formulation maintained fully subambient temperatures over a 24-h period considering a 5-min running average, with an average temperature reduction of 1.97 °C. Ultimately, the proposed hBN MP-101 formulation offers a hydrophobic, strong, UV-resistant, and easily applicable paint with the highest reflectance among hydrophobic radiative cooling paints.

METHODS

Paint Fabrication

The fabrication of the paint was designed to closely resemble that of a commercial process to make it easy to scale the paint to a manufactured level. The first step was to weigh out the three base ingredients of the paint: the binder, MP-101; the pigment, hexagonal boron nitride (hBN); and the solvent, dimethylformamide (DMF). For hBN, a particle distribution size of 332 ± 193 nm was used, based on previous optimization efforts.[15] The exact ratio of these ingredients was expressed as the pigment loading: for instance, if the pigment loading of a sample is 60%, then the hBN would comprise 60% of the final dry solid volume, and the MP-101 would make up the remaining 40% of the solid volume. The volume of solvent needed for this formulation was approximately ten times the amount of MP-101, but this amount can vary based on pigment loading (more pigment needs more solvent) and final desired viscosity (more solvent leads to lower viscosity). Multiple pigment loadings were made and studied to optimize the paint's properties.

Once the materials were weighed, MP-101 and DMF were mixed until separation could no longer be observed. Then the pigment was added to the mixture, and the paint was sonicated until the pigment particles were fully suspended in the matrix. Once the paint was created, it was plated onto a suitable substrate for the corresponding measurement.

Density and Surface Wettability Characterization

The hydrophobicity of the paint was characterized by SEM images and porosity calculations to better understand the structure at a microscale level. The SEM images were taken on an FEI Nova NanoSEM at varying magnifications. The porosity (ϕ_P) of the dried paint layer was calculated using the following equation, using the 83% pigment solid volume fraction as an example:

$$\phi_P = 1 - \phi_S = 1 - \frac{\rho_{paint}}{0.83 \times \rho_{hBN} + 0.17 \times \rho_{MP\text{-}101}} \quad (2)$$

where ϕ_S is the solid fraction and 0.83 and 0.17 are the respective solid volume fractions of the hBN pigment and MP-101 binder, corresponding to an 83% pigment volume concentration.

To check whether the paint is self-cleaning, static and dynamic water droplet contact angle tests were performed to characterize the hydrophobicity of the material. For static testing, a 10 μL water drop was placed carefully on top using the Ramé-hart 100-22 automated dispensing system, and a camera was positioned to view the side of this drop. A picture was taken, and the angle that the water creates with the sample was measured with a Ramé-hart 290-F1 goniometer. Then, dynamic testing was completed using the process outlined in the Results and Discussion section once again using the Ramé-hart 100-22 automated dispensing system and the Ramé-hart 290-F1 goniometer.

Optical Measurements

Next, the optical properties of the new formulation were characterized by using a Lambda 950 UV−vis−NIR as well as a Nicolet iS50 FT-IR spectrometer to understand its overall impact on the cooling effect. With these spectrometers, the spectral transmission, reflection, and absorption were characterized across wavelengths from 250 nm to 20 μm (250 nm−2.5 μm with UV−vis−NIR spectrometry and 2.5−20 μm with FTIR spectrometry). Following this, the spectral properties were used together with the AM 1.5 solar irradiation spectra to calculate the normalized total solar reflectance, transmittance, and absorptance as well as emittance within the sky window. These results were then compared to past formulations and modeled optical properties.

To find the refractive index (n) and extinction coefficient (κ), a plain sample of MP-101 with a 1.27 mm thickness was plated on a

https://doi.org/10.1021/acsaom.5c00079
ACS Appl. Opt. Mater. XXXX, XXX, XXX−XXX

glass slide as well as a plain sample of acrylic. Once dried, the two samples were placed in a Lambda 950 UV/vis spectrometer to gain a fundamental understanding of their optical properties. n and κ for the MP-101 binder were calculated first by using spectrometry to measure the absorptivity, reflectivity, and transmissivity from 0.25 to 20.00 μm. κ was then calculated using the following process from David Look's work:[34]

$$x_1 = \frac{(1-R)^2 - t^2}{2t} \times \left(1 + \frac{4t^2}{((1-R)^2 - t^2)^2}\right)^{0.5} - 1 \quad (3)$$

$$\alpha = \frac{1}{d} \times \ln\left(\frac{1}{x_1}\right) \quad (4)$$

$$\kappa = \frac{\lambda \times \alpha}{4\pi} \quad (5)$$

where d is the thickness in nm, λ is the wavelength in nm, R is the reflectance, t is the transmission coefficient, and n was calculated using the following process:

$$n = \frac{1+R}{1-R} + \left(\frac{4R}{(1-R)^2} - R^2\right)^{0.5} \quad (6)$$

with

$$R = \frac{r}{1 + T - x_1} \quad (7)$$

where T is the transmittance.

Strength and Weathering Measurements

To further characterize the capabilities of the paint, exposure weathering was conducted, as explained in the Results and Discussion section. More information about the standard used (ISO 11341, Cycle A, Method 1) can be found in Table S4. Due to time and cost constraints, the time measured was up to 250 h of advanced exposure, as opposed to the ISO standard's maximum recommended time of 1000 h, which is a common reduction with this standard.[35−38]

Outdoor Measurements

For the outdoor testing, samples were elevated off the roof by a 3-ft-tall metal table and then further insulated from potential conduction issues with a layer of foam covered by aluminum foil, hollow paper stilts, and one more layer of stilts within a sample holder also made of foam covered in aluminum foil. The sample holder was designed to be close to the edge of the sample without touching the sample to again reduce conduction. A convection shield was either built on top of the sample with LDPE (as shown in Figure 3a) or as "walls" around the entire sample holding mechanism with wooden poles and thin cling wrap (as shown in Figure S4). Thermocouples were attached on the underside of the sample, within the cell but not touching the sample, as well as outside of the holder ("ambient" air) in an ambient house to minimize direct radiation exposure. Tests were conducted on clear, low-humidity days from 9/13/2023 to 9/15/2023 to maximize the cooling effect of the paint.

ASSOCIATED CONTENT

Supporting Information

The Supporting Information is available free of charge at https://pubs.acs.org/doi/10.1021/acsaom.5c00079.

Additional SEM imaging, full optical spectrum for acrylic and MP-101, individual spectral measurements for six pigment loadings, topcoat study results, additional outdoor testing method, sky window emission for different pigment loadings, exact data for Figure 3b, exact data for Figure 5a, parameters for the weathering test, and a video of the hydrophobic capability of the paint (PDF)

AUTHOR INFORMATION

Corresponding Author

Xiulin Ruan − *School of Mechanical Engineering, Purdue University, West Lafayette, Indiana 47906, United States; Birck Nanotechnology Center, Birck Nanotechnology Center, Purdue University, West Lafayette, Indiana 47906, United States;* orcid.org/0000-0001-7611-7449; Email: ruan@purdue.edu

Authors

Emily Barber − *School of Mechanical Engineering, Purdue University, West Lafayette, Indiana 47906, United States;* orcid.org/0009-0003-6294-7152

Dudong Feng − *School of Mechanical Engineering, Purdue University, West Lafayette, Indiana 47906, United States*

Ziqi Fang − *School of Mechanical Engineering, Purdue University, West Lafayette, Indiana 47906, United States*

Daniel Carne − *School of Mechanical Engineering, Purdue University, West Lafayette, Indiana 47906, United States;* orcid.org/0009-0009-1531-8189

Orlando Rivera Gonzalez − *School of Mechanical Engineering, Purdue University, West Lafayette, Indiana 47906, United States*

Won-June Lee − *James Tarpo Jr. and Margaret Tarpo Department of Chemistry, Purdue University, West Lafayette, Indiana 47907, United States;* orcid.org/0000-0001-8756-0956

Navdeep Vansal − *School of Mechanical Engineering, Purdue University, West Lafayette, Indiana 47906, United States*

Katherine Raykova − *School of Mechanical Engineering, Purdue University, West Lafayette, Indiana 47906, United States*

Complete contact information is available at: https://pubs.acs.org/10.1021/acsaom.5c00079

Author Contributions

Conceptualization: X.R., E.B.; methodology: E.B., D.F., X.R.; investigation: E.B., D.F., Z.F., D.C. O.R.G., W.-J.L., N.V., K.R.; writing (original draft): E.B.; writing (review and editing): X.R., E.B., D.F.; resources: X.R., J.M.; and supervision: X.R. The manuscript was written with contributions from all authors. All authors have approved the final version of the manuscript.

Notes

The authors declare the following competing financial interest(s): X.R. and E.B. are the inventors of an international patent application (WO2024118766A1) filed on November 29, 2023 on the basis of the work described here.

ACKNOWLEDGMENTS

E.B. acknowledges support from the US National Science Foundation through a Graduate Research Fellowship. X.R., D.F., and D.C. acknowledge partial support from the US National Science Foundation through award 2102645 and the Trask Fund at Purdue University. Z.F. acknowledges support from Purdue University through a teaching assistantship. O.R.G. acknowledges the National Science Foundation for support under the Graduate Research Fellowship Program (GRFP) under grant number DGE-1842166. W.-J.L. acknowledges support from Ambilight Inc. under contract No. 4000187.02. N.V. and K.R. acknowledge support through the

Purdue University SURF program. The authors acknowledge Dr. Jianguo Mei for providing his laboratory space and Q-SUN XE-3 instrument.

ADDITIONAL NOTE

[a]Notably, the reflectance is explored here instead of emissivity due to its overwhelming contribution to the cooling power of the paint, as noted in previous work.

REFERENCES

(1) Mayclin, D. *Air Conditioning Accounts For About 12% Of U.S. Home Energy Expenditures*. U.S. EIA https://www.eia.gov/todayinenergy/detail.php?id=36692, 2018.
(2) U.S. EIA. *Frequently Asked Questions: What is U.S. Electricity Generation by Energy Source?* https://www.eia.gov/tools/faqs/faq.php?id=427&t=3# 2022.
(3) Robert, B. *The PROCESS of making ICE in the East-Indies. By Sir Robert Barker, F. R. S. in a Letter to Dr. BROCKLESBY*; ProQuest, 1776.
(4) Times Of India *The mystery behind blue and white houses of Greece*; Times Of India, 2019.
(5) Harrison, A. W.; Walton, M. R. Radiative cooling of TiO2 white paint. *Sol. Energy* **1978**, *20*, 185−188.
(6) Michell, D.; Biggs, K. L. Radiation cooling of buildings at night. *Appl. Energy* **1979**, *5*, 263−275.
(7) Raman, A. P.; Anoma, M. A.; Zhu, L.; Rephaeli, E.; Fan, S. Passive radiative cooling below ambient air temperature under direct sunlight. *Nature* **2014**, *515*, 540−544.
(8) Kou, J.; Jurado, Z.; Chen, Z.; Fan, S.; Minnich, A. J. Daytime Radiative Cooling Using Near-Black Infrared Emitters. *ACS Photonics* **2017**, *4*, 626−630.
(9) Bao, H. Double-layer nanoparticle-based coatings for efficient terrestrial radiative cooling. *Sol. Energy Mater. Sol. Cells* **2017**, *168*, 78−84.
(10) Huang, Z.; Ruan, X. Nanoparticle embedded double-layer coating for daytime radiative cooling. *Int. J. Heat Mass Transfer.* **2017**, *104*, 890−896.
(11) Mandal, J.; Yang, Y.; Yu, N.; Raman, A. P. Paints as a Scalable and Effective Radiative Cooling Technology for Buildings. *Joule* **2020**, *4*, 1350−1356.
(12) Atiganyanun, S.; Plumley, J. B.; Han, S. J.; Hsu, K.; Cytrynbaum, J.; Peng, T. L.; Han, S. M.; Han, S. E. Effective Radiative Cooling by Paint-Format Microsphere-Based Photonic Random Media. *ACS Photonics* **2018**, *5*, 1181−1187.
(13) Li, X.; Peoples, J.; Huang, Z.; Zhao, Z.; Qiu, J.; Ruan, X. Full Daytime Sub-ambient Radiative Cooling in Commercial-like Paints with High Figure of Merit. *Cell Rep. Phys. Sci.* **2020**, *1*, 100221.
(14) Li, X.; Peoples, J.; Yao, P.; Ruan, X. Ultrawhite BaSO4 Paints and Films for Remarkable Daytime Subambient Radiative Cooling. *ACS Appl. Mater. Interfaces* **2021**, *13*, 21733−21739.
(15) Felicelli, A.; Katsamba, I.; Barrios, F.; Zhang, Y.; Guo, Z.; Peoples, J.; Chiu, G.; Ruan, X. Thin layer lightweight and ultrawhite hexagonal boron nitride nanoporous paints for daytime radiative cooling. *Cell Rep. Phys. Sci.* **2022**, *3*, 101058.
(16) Song, J.; Zhang, W.; Sun, Z.; Pan, M.; Tian, F.; Li, X.; Ye, M.; Deng, X. Durable radiative cooling against environmental aging. *Nat. Commun.* **2022**, *13*, 4805.
(17) Bretz, S. E.; Akbari, H. Long-term performance of high-albedo roof coatings. *Energy Build* **1997**, *25*, 159−167.
(18) Cool Roof Rating Council. *Roof Product Directory*. https://coolroofs.org/directory/roof?orderBy=initial_SRI&sort=desc.
(19) Liu, S.; Zhang, F.; Chen, X.; Yan, H.; Chen, W.; Chen, M. Thin paints for durable and scalable radiative cooling. *J. Energy Chem.* **2024**, *90*, 176−182.
(20) Zuo, T. "Cherimoya-like" polysilsequioxane microspheres with structure-enhanced spectral capability for passive daytime radiative cooling. *Mater. Today Commun.* **2022**, *32*, 104096.
(21) Jiang, T.; Fan, W.; Wang, F. Long-lasting self-cleaning daytime radiative cooling paint for building. *Colloids Surf.* **2023**, *666*, 131296.
(22) Tian, Y. Superhydrophobic and Recyclable Cellulose-Fiber-Based Composites for High-Efficiency Passive Radiative Cooling. *ACS Appl. Mater. Interfaces* **2021**, *13*, 22521−22530.
(23) Liu, J.; Ma, W.; Deng, X.; Cai, H. Superhydrophobic nanoparticle mixture coating for highly efficient all-day radiative cooling. *Appl. Therm. Eng.* **2023**, *228*, 120490.
(24) Jiang, T. All-Polymer Superhydrophobic Radiative Cooling Coating Based on Polytetrafluoroethylene/Polydimethylsiloxane Composites. *Ind. Eng. Chem. Res.* **2023**, *62*, 5024−5034.
(25) Nie, S.; Tan, X.; Li, X.; Wei, K.; Xiao, T.; Jiang, L.; Geng, J.; Liu, Y.; Hu, W.; Chen, X. Facile and environmentally-friendly fabrication of robust composite film with superhydrophobicity and radiative cooling property. *Compos. Sci. Technol.* **2022**, *230*, 109750.
(26) Lio, G. E.; Werlé, J.; Arduini, M.; Wiersma, D. S.; Manara, J.; Pattelli, L. Radiative Cooling Potential of a Water-Based Paint Formulation under Realistic Application Conditions. *ACS Appl. Opt. Mater.* **2024**, *2*, 2459−2468.
(27) Xue, C. H.; Wei, R.-X.; Guo, X.-J.; Liu, B.-Y.; Du, M.-M.; Huang, M.-C.; Li, H.-G.; Jia, S.-T. Fabrication of superhydrophobic P(VDF-HFP)/SiO2 composite film for stable radiative cooling. *Compos. Sci. Technol.* **2022**, *220*, 109279.
(28) Wang, H. D.; Xue, C.-H.; Guo, X.-J.; Liu, B.-Y.; Ji, Z.-Y.; Huang, M.-C.; Jia, S.-T. Superhydrophobic porous film for daytime radiative cooling. *Appl. Mater. Today* **2021**, *24*, 101100.
(29) Zhang, S. Full daytime sub-ambient radiative cooling film with high efficiency and low cost. *Renew. Energy* **2022**, *194*, 850−857.
(30) Cheng, Z.; Han, H.; Wang, F.; Yan, Y.; Shi, X.; Liang, H.; Zhang, X.; Shuai, Y. Efficient radiative cooling coating with biomimetic human skin wrinkle structure. *Nano Energy* **2021**, *89*, 106377.
(31) Orel, B.; Gunde, M. K.; Krainer, A. Radiative cooling efficiency of white pigmented paints. *Sol. Energy* **1993**, *50*, 477−482.
(32) Feng, L. Petal effect: A superhydrophobic state with high adhesive force. *Langmuir* **2008**, *24*, 4114−4119.
(33) Sengupta, M. The National Solar Radiation Data Base (NSRDB). *Renewable Sustainable Energy Rev.* **2018**, *89*, 51−60.
(34) Look, D. C.; Leach, J. H. On the Accurate Determination of Absorption Coefficient from Reflectance and Transmittance Measurements: Application to Fe-Doped GaN. *J. Vac. Sci. Technol. B* **2016**, *34*, 04J105.
(35) Tsvetkova, N. N.; Pas'ko, Y. V.; Tsvetkov, V. E.; Ugryumov, S. A. Operational Properties of Imported and Domestic Paints and Varnishes. *Polymer Science - Series D* **2020**, *13*, 424−428.
(36) Karlessi, T.; Santamouris, M. Improving the performance of thermochromic coatings with the use of UV and optical filters tested under accelerated aging conditions. *Int. J. Low-Carbon Technol.* **2015**, *10*, 45−61.
(37) Huang, Y.; Zhang, J.; Wang, Z.; Liu, Y.; Wang, P.; Cao, J.-J.; Ho, W. g-C3N4/TiO2 Composite Film in the Fabrication of a Photocatalytic Air-Purifying Pavements. *Sol. RRL* **2020**, *4*, 2000170.
(38) Žigon, J.; Pavlič, M.; Petrič, M.; Dahle, S. Surface properties of coated MDF pre-treated with atmospheric plasma and the influence of artificial weathering. *Mater. Chem. Phys.* **2021**, *263*, 124358.

https://doi.org/10.1021/acsaom.5c00079
ACS Appl. Opt. Mater. XXXX, XXX, XXX−XXX